The Importance of Pulsatile Microcirculation in Relation to Hypertension

Studying the Relationship Between Abdominal Aortic Blood Pressure and Renal Cortex Flux

Ming-Yie Jan[1,2], Hsin Hsiu[1,2], Tse-Lin Hsu[2], Yuh-Ying Lin Wang[3], Wei-Kung Wang[1,2]
[1]Department of Electrical Engineering, National Taiwan University
[2]Biophysics Lab., Institute of Physics, Academia Sinica, Taipei
[3]Department of Physics, National Taiwan Normal University

Hypertension is one of the most common and lethal diseases in developed countries. Elevated blood pressure can increase the load of the heart and cause stroke, arterial arteriosclerosis, coronary artery disease, and many other arterial diseases. Only less than 10% of hypertension cases are secondary, while over 90% are primary (or "essential") [1]. Essential hypertension (EH) is related to many factors such as environmental, genetic, and even nutritional aspects: its causes are complex and hard to ascertain. Considering constant cardiac output, induced high blood pressure is mainly related to elevation of blood-vessel resistance, especially those of the peripheral vascular beds (PVBs).

The aim of the study presented in this article was to prove that increased pulsatile blood pressure (PBP) increases perfusion in PVBs. We used a laser Doppler flowmeter (LDF) to measure surface renal cortical flux (RCF) and a pressure-tip transducer catheter to measure abdominal aortic blood pressure (AABP). Besides demonstrating the relationship between RCF and AABP by linear regressive analysis with an averaged periodogram (AP), we also used time-domain pulse averaging to clarify the pulsatile AABP and RCF. Furthermore, we define a flux-to-pressure-area ratio (FPAR) to evaluate the efficiency by which the pulsatile AABP drives RCF.

Understanding Blood Pressure

It is known that the mean blood pressures (MBP) measured in the aorta, the arteries, and even the small arteries are almost constant but drop abruptly in the regions where arterioles (outer diameter < 40 μm) distribute to numerous capillaries [2, 3]. This phenomenon implies that PVBs are the principal site of regulating the energy transformation to provide blood flow. In those regions, part of the pressure drop is caused by frictional loss and the other part is the driving force of blood flow to the microvessels. Both blood viscosity and blood-flow mechanics in PVBs have been reviewed [4, 5, 6]; they depend mainly on the driving force and the diameter of the blood vessels. As the blood-flow driving force increases, red blood cells (RBCs) will be deformed. This deformation can break up cell interlinkings as well as disassociate RBC aggregation within a characteristic short time (0.06 sec or less) [5, 7, 8]. Meanwhile, increased diameter of an upstream vessel can accelerate the RBC velocity in the downstream vessels in PVBs [6, 9].

When the heart contracts, aortic dilatation changes kinetic energy of the blood into potential energy. Pressure wave propagation in the aorta can be quantitatively described by an arterial model with radial dilatation [10]. Moreover, according to coupled resonance theory [11], the connected elastic vascular beds redistribute the pressure wave. Finally, we had proposed pressure distribution equations and proved that the coupled pressure in an elastic vascular bed drives the flow in the end-outlet of a simulated tree-like vascular model [12].

In our previous research [12-15], we showed that the fast-propagating blood pressure wave generated by cardiac contraction drives pulsatile blood flow coherently in PVBs. From the aorta to the PVBs, the pulsatile pressure simulta-

Table 1. Basic Physiological Parameters

	Rat 1	Rat 2	Rat 3	Rat 4	Rat 5	Rat 6
Weight (g)	368	250	295	380	350	310
Number of Measured Sites	3	4	3	3	2	2
Number of Selected Sites	3	4	2	2	1	1
Heart Rate (Hz)	5.11 ± 0.05	7.30 ± 0.19	7.17 ± 0.05	6.72 ± 0.55	6.03	7.8
Mean Blood Pressure (mmHg)	94.18 ± 1.11	92.33 ± 1.51	93.6 ± 0.71	93.6 ± 3.68	90.8	94.4
Pulsatile Blood Pressure (Diastolic to Systolic Value)	53.58 ± 1.67	68.4 ± 5.97	43.4 ± 0.42	47.65 ± 0.07	51.5	43.9
Mean Flux (Units)	156.48 ± 4.36	99.00 ± 5.67	98.05 ± 7.14	152.95 ± 7.28	128.7	129.5

 0739-5175/00/$10.00©2000IEEE

Authorized licensed use limited to: National Taiwan University. Downloaded on August 02,2022 at 06:45:49 UTC from IEEE Xplore. Restrictions apply.

neously drives blood flow. Closer to the PVBs, vessels become more rigid and resistance-like; thus, steadier pulsatile flow in the PVBs replaces the upstream coupled pressure wave of the elastic vascular beds. Other fluctuations of flow in the PVBs have been reported, but they are much slower than the pulsatility created by the heart [16].

Mean transient time (MTT) of blood flow from the aorta to PVBs is a few seconds [17]. Although the pulsatility was once assumed to be completely damped to produce a steady flow in the microvessels [18, 19], it has been demonstrated in some studies that pulsatility exists in the arterioles, the precapillary arterioles, the capillaries, and even the postcapillary venules [2, 18-20]. However, until now, the role of the pulsatility in the PVBs was not clearly understood.

As the PBP wave propagates to the PVBs, a high peak force can dilate the precapillary opening. The wider opening reduces resistance and thus further increases the driving force to the PVBs. Moreover, the increased driving force can deform the RBCs and other blood cells so as to change cell-to-cell interactions. It can also lower blood viscosity as well as dissociate RBC aggregations [21, 22]. The driving pulsatile pressure associated with dilation of precapillary openings and the reduction of blood viscosity could play an important role in the delivery of blood flow Q to the PVBs:

$$Q = V(r,\eta) \times A(r)$$

where blood velocity V depends directly on the radius r of the precapillary opening and inversely on the blood viscosity η. The cross-sectional area A of the blood vessel is also directly related to the radius of the opening.

Materials and Methods

Animal Preparation and Experimental Setup

This investigation conformed with the "Guide for the Care and Use of Laboratory Animals" published by the US National Institutes of Health (NIH Publication No. 85-23, revised 1985).

Six male Sprague-Dawley rats were anesthetized with Urethane (700mg/kg ip) and placed on a heated pad to maintain body temperature. The AABP was recorded (by cannulating) from the caudal artery to the abdominal aorta with a catheter-tip pressure transducer (P10EZ, Viggo-Spectramed, USA).

A laser Doppler flowmeter (Model MBF3, Moor Instruments Ltd., England) was used for the measurement of RCF (time constant 0.05 sec, 14.9 kHz cutoff). The LDF uses the Doppler shift of back-scattered laser light to estimate RBC velocity. The measured flux was equal to $\bar{v} \times C$, where $\bar{v}$ is the mean velocity of the measured RBCs and C is the concentration of the moving RBCs in the measured tissue [23]. An optical-fiber probe (P10M+P17, plastic fiber 500 μ O.D., Moor Instruments Ltd.) was calibrated with a flux standard (Moor Instruments Ltd.) to ensure its stability and performance. The left kidney was exposed on the dorsal side of the rat, fixed with cotton balls, and then the fatty capsule was carefully separated. The optical-fiber probe was fixed vertically and gently touched on the surface of renal cortex. Due to the tiny momentum in PVBs, the force that the probe exerts on the surface of renal cortex should be very tiny so as not to disturb the measurement. In this study, it is about 0.5-1.0 mN; when it is over 10 mN, the measured pulsatility would diminish and then disappear.

Employing back-scattering light, LDF has the least effect on tissue preparation that would affect propagation of the pulsatility.

The signal due to respiration can be easily detected because its period is three to five times that of the heartbeat; proper installation of the probe and good care of the animals during the experiments can reduce this extraneous signal. While the experiments were under way, the surface of the kidney was bathed with a 37°C normal saline solution to keep it from drying. Systolic and diastolic aortic blood pressure were monitored throughout the experiments. The microcirculation flux signal was recorded from the analog out-

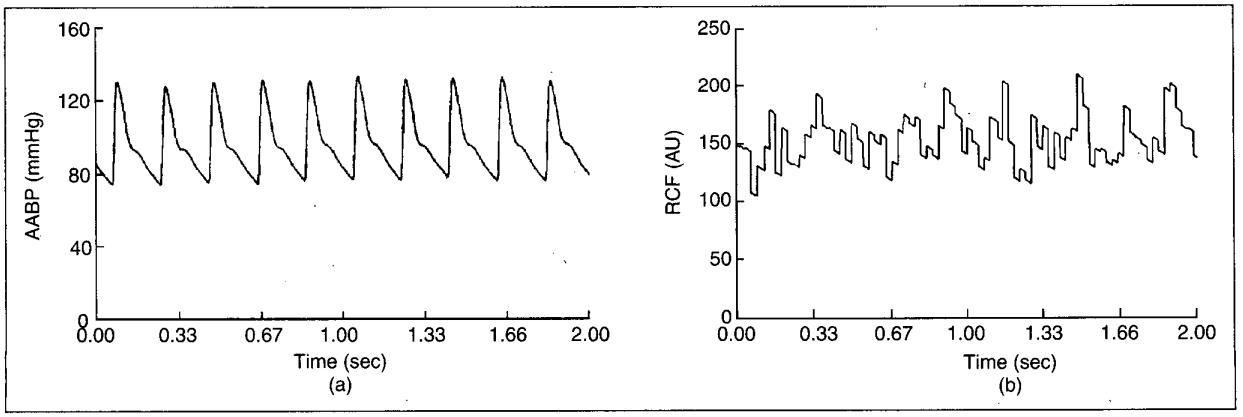

1. Plots of 2 sec raw data sampled by the experimental setup: (a) abdominal aortic blood pressure (AABP) and (b) renal cortical flux (RCF), measured simultaneously.

Authorized licensed use limited to: National Taiwan University. Downloaded on August 02,2022 at 06:45:49 UTC from IEEE Xplore. Restrictions apply.

put of the LDF. Both AABP and RCF signals were sent to a simultaneous sample-and-hold card AX753 (AXIOM Technology Co., LTD. Taiwan, R.O.C.), and then to an A/D converter card AX5621 (AXIOM Technology) with 1500 Hz sampling rate. At least two sites on the renal cortex were measured in each rat, and all the measurement sites were chosen away from any visible vessels. At each site, 32 data sequences, each containing 2 sec signals, were acquired by a 486-based personal computer. The data sequence recorded 8-14 pulses, depending on the heart rate of the rat.

Signal Processing

Averaged Periodogram

As the LDF signal is noisy, a highly selective signal processing technique is necessary to extract the desired information. A classical averaged periodogram was employed to enhance the signal-to-noise ratio (SNR). This estimation method, based on the fast Fourier transform (FFT), analyzes the power spectral density (PSD) function so that we can understand the frequency structures of RCF and AABP.

On each site, we recorded a 64 sec continuous signal. The period of each pulse was determined by the two lowest points of the blood-pressure pulse. In each sequence, the mean and the coefficient of variance (CV = SD/mean) of the heart rates was calculated. Two criteria were employed to verify a stable sequence to be averaged: (1) The CV of the heart rate of a sequence was under 2%; and (2) the mean heart rate of a sequence varied no more than 2% from the mode of the mean measured heart rate (at that site). Only sequences that satisfied both criteria were used in the analysis. By subtraction of the mean of each selected data sequence, the remaining pulsatile component was denoted as $x^{(p)}[n]$, where p is the pth selected sequence in each set. Each data sequence contained $N = 3000$ points, with a 1500 Hz sampling rate.

Since K independent data sequences were selected at each measured site, an averaged periodogram estimator is defined as

$$\hat{P}_{\mathrm{AVEPER}}[f] = \frac{1}{K}\sum_{p=0}^{K-1}\hat{P}_{\mathrm{PER}}^{(p)}[f],$$

where $\hat{P}_{PER}^{(p)}[f]$ is the periodogram of the pth data sequence:

$$\hat{P}_{\mathrm{per}}^{(p)}[f] = \frac{1}{N}\left|\sum_{n=0}^{N-1}x^{(p)}[n]\exp(-j2\pi fn)\right|^2.$$

To have finer frequency spacing and to more closely estimate the periodogram, each data sequence was padded with 5192 zeros to create an 8192-point FFT. No extra resolution was afforded by this padding, but a better evaluation of the periodogram resulted. With the averaged periodogram, the variance is decreased by a factor of K since each sampled sequence is independent, and

$$\mathrm{var}\left[\hat{P}_{\mathrm{AVEPER}}[f]\right] = \frac{1}{K}\mathrm{var}\left[\hat{P}_{\mathrm{PER}}^{(p)}[f]\right].$$

Estimation of Pulsatile Components

The pulsatile components generally reflect the dynamic properties of a system. In this study, we evaluated the efficiency of the pulsatile driving pressure (AABP) in driving the local blood flux (RCF) over

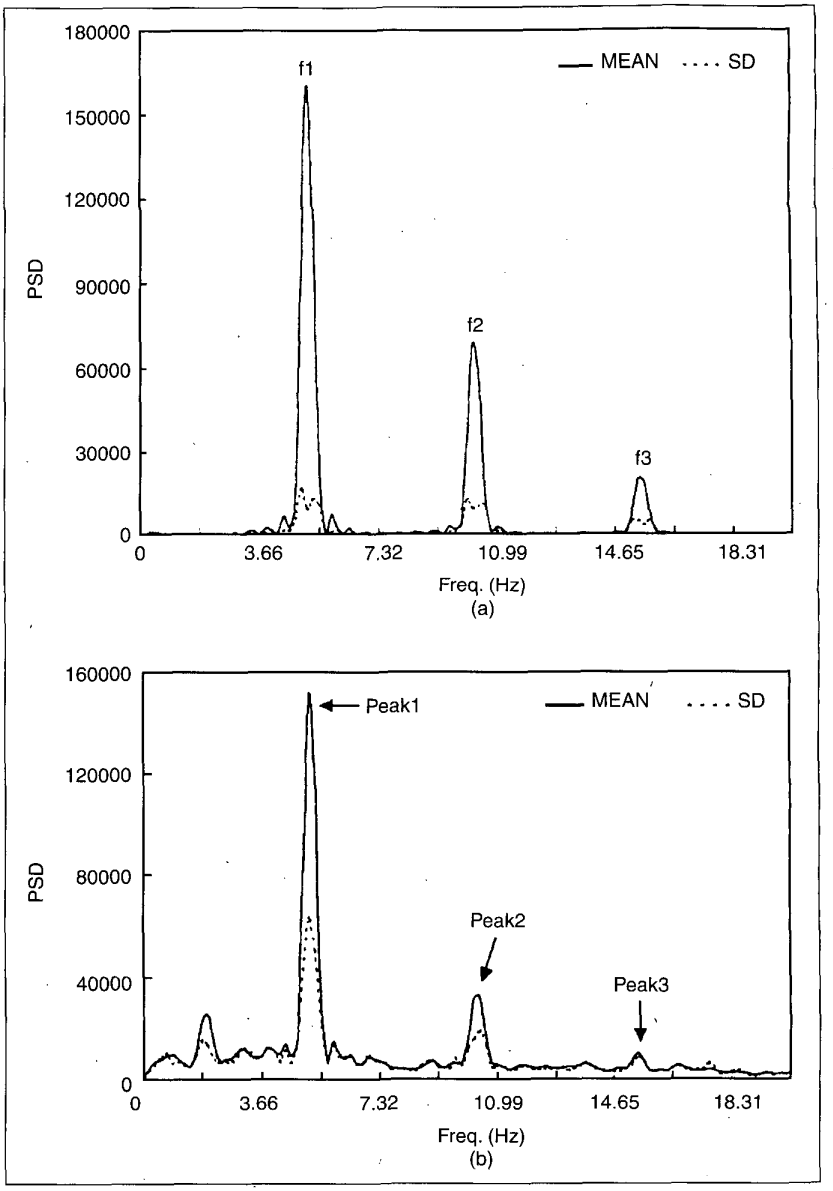

2. The averaged periodogram (AP) with 12 selected sequences that satisfied the two selection criteria stated in the text. The solid line is the AP, and the dashed line is its standard deviation (SD). (a) AABP. The values f_i, $i = 1 \sim 3$ denote the harmonics of the fundamental heart rate. (b) RCF. (Definitions of the peak frequencies $f_{RCF}(i)$ are given in text.)

Authorized licensed use limited to: National Taiwan University. Downloaded on August 02,2022 at 06:45:49 UTC from IEEE Xplore. Restrictions apply.

one cardiac cycle. To elucidate the pulsatile component of RCF, we used time-domain pulse averaging to enhance the SNR. The cardiac cycle was determined by the two relative lowest values of AABP, and a corresponding cycle of RCF was also determined. The averaged pulse was then defined as:

$$x_{\text{ave}}[n] \quad \frac{1}{M} \sum_{m \ 1}^{M} x_m[n].$$

To enhance SNR, we used at least M = 150 pulses to estimate the averaged pulse. The pulsatile component $x_{\text{ave}}^{\text{pul}}[n]$ is defined as the averaged pulse minus the diastolic value:

$$x_{\text{ave}}^{\text{pul}}[n] \quad x_{\text{ave}}[n] - dias(x_{\text{ave}}[n]).$$

Pulsatile components of both AABP and RCF were estimated and then normalized to the same scale. According to the relative magnitude, the averaged pulses were divided into four parts: I (7500-10000), II (5000-7500), III (2500-5000), and IV (0-2500). The area of each part, representing the cumulated quantity, was calculated. The flux-to-pressure-area ratio $FPAR_X$ was defined as the ratio of the area of RCF_X divided by the corresponding area of $AABP_X$ (where x represents averaged pulses: I, II, III, and IV). Meanwhile, on each site, a blood-pressure pulsatile index (BPPI), defined as (systolic pressure – diastolic pressure)/diastolic pressure was evaluated. Signal processing was performed with the IBM-PC version of MATLAB (Math Works, Natick, MA).

Statistical Analysis

Linear regressive analysis was used to identify the frequency relationship of the structure between RCF and AABP. Let the first harmonic of the fundamental heart rate be f_1 and the ith harmonics be $f_i \quad i \quad f_1$. Thus, we define the peak frequencies $f_{\text{RCF}}(i)$ of RCF as the frequencies of the maximum PSD in the frequency intervals $f_i \quad 1/2f_1$, for $i \quad 1,2,3$, respectively.

Results

The basic physiological parameters of the experiments are listed in Table 1. There are 13 selected sites, and at each site at least 12 data sequences satisfying the two designated criteria are chosen. The heart rate, MBP, PBP, mean flux, and pulsatile flux are calculated for the selected sites.

Table 2. The Linear Regressive Analysis Between RCF Peaks and AABP Peaks (n = 13)

	Peak 1	Peak 2	Peak 3*
Correlation Coeff.	1	0.999	0.999
Slope	1	1	1.002

$p < 0.001$, * n = 5

Figure 1 demonstrates the 2 sec samples of the raw data sequences of AABP [Fig. 1 (a)] and RCF [Fig. 1 (b)]. It seems that RCF is roughly pulsatile and synchronized with AABP. Figure 2 shows a sample of AP (solid line) and its standard deviation (dashed line) in which 12 periodograms are averaged. Figure 2(a) clearly shows that only the harmonics of the heartbeat exist within AABP, and Fig. 2(b) shows that the peaks of the averaged periodogram of RCF follow the harmonics of AABP. Table 2 gives the results of the linear regressive analysis between the first three peaks of RCF and the first three harmonics of AABP. Due to the limitation of the sampling rate of the LDF signal, there are only five sites that can be resolved up to the third harmonic. The same result, that RCF is pulsatile, was also shown in our previous study on dogs [15].

Figure 3(a) shows a sample of the time-domain pulse averaging; there are eight selected sites with more than 150 pulses to be averaged. The pulsatile components of the averaged pulses of AABP (solid line) and RCF (dashed line) are normalized to the same scale, as shown in Fig. 3(b) (based on relative magnitudes, they are divided into four categories, as descried above). The areas of the four parts of both RCF and AABP are calculated to determine their corresponding FPAR. FPAR I, FPAR II, FPAR III, and FPAR IV are the ratios that correspond to the areas of the four parts from peak to bottom, respectively. The corresponding BPPI of every site is also calculated.

The plot of FPAR versus BPPI of the eight selected sites is illustrated in Fig. 4. Table 3 demonstrates the characteristics of FPARs versus BPPI; it shows that FPARs of the higher parts are larger than that of the lowest parts. Moreover, there exists a threshold of BPPI (BPPI = 0.69) at which FPAR increases abruptly. As BPPI is beyond the threshold, the FPARs of the higher components increase abruptly, but the FPAR of the lowest component is still kept in a constant range (Table 3; slopes = 1.67, 1.08, 0.79, –0.04, and n = 5 for FPAR I, FPAR II, FPAR III, and FPAR IV, respectively).

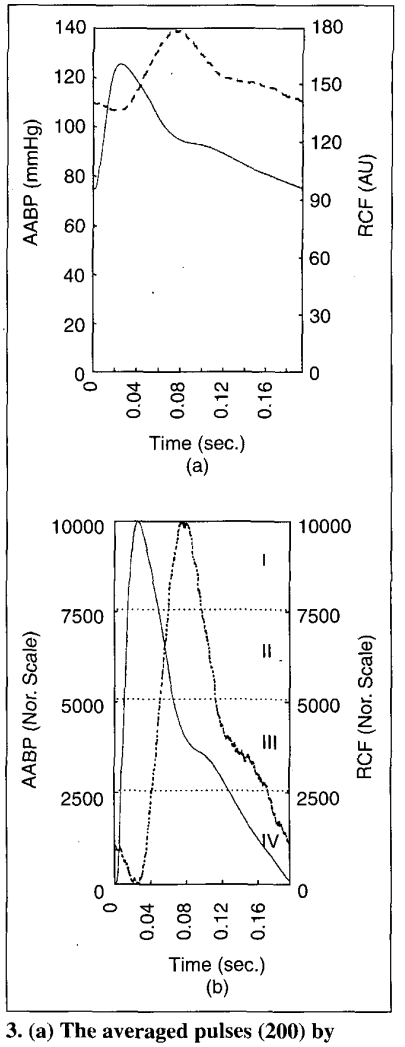

3. (a) The averaged pulses (200) by time-domain pulse averaging. (b) The normalized pulses are divided into four categories according to the normalized scale: I (7500-10000), II (5000-7500), III (2500-5000), and IV (0-2500). The solid line is AABP, and the dashed line is RCF in both figures.

Authorized licensed use limited to: National Taiwan University. Downloaded on August 02,2022 at 06:45:49 UTC from IEEE Xplore. Restrictions apply.

Table 3. Characteristics of FPARs				
	FPAR I	FPAR II	FPAR III	FPAR IV
Mean ± SD of FPAR below the threshold (BPPI ≤ 0.69, n=4)*@	1.15 ± 0.05	1.18 ± 0.03	1.11 ± 0.02	1.05 ± 0.04
Slope of FPAR above the threshold (BPPI ≥ 0.69, n = 5)	1.67	1.08	0.79	–0.04
*FPAR I and FPAR II are significantly larger than FPAR IV ($P < 0.05$) @FPAR III is larger than FPAR IV ($P < 0.1$)				

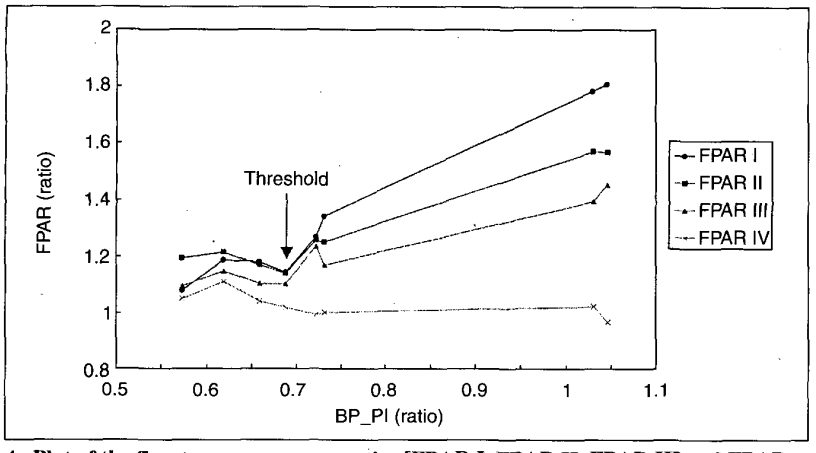

4. Plot of the flux-to-pressure-area ratios [FPAR I, FPAR II, FPAR III and FPAR IV, according to the four parts in Fig. 3(b)] versus the blood-pressure pulsatile index (BPPI). The FPARs of the higher parts are larger than that of the lowest part. Moreover, as BPPI is larger than 0.69 (a threshold), the FPARs of higher parts increase abruptly. The FPAR of the lowest part remains in a constant range.

Discussion

According to Bonner's model [23], the LDF measures the nondirectional velocity of numerous RBCs in the randomly distributed blood vessels. If the RBCs are not coherently driven by the fast-propagating blood-pressure wave, the flow could not be in phase and would not be measured to be pulsatile. Due to the relatively very small mechanical force in PVBs, the measurement of pulsatile flow in the microcirculation should be with as few perturbations as possible. The structure of a solid organ could support an external load, but too large an external load would diminish the pulsatility. Employing back-scattering light, LDF has the advantage of having the least effect on tissue preparation that would affect propagation of the pulsatility. The results shown in Figs. 1 and 2 and Table 2 show that RCF is driven by the pulsatile aortic blood pressure, which is coincident with the conclusion of our previous study [15].

The most important results of this research are shown in Fig. 4. First, in the region where BPPI is smaller than 0.69, FPARs in the higher parts of the averaged pulses are larger than that in the lower part (Fig. 4 and Table 3). This indicates that the pulsatile pressure peak can drive flux more effectively in PVBs. This phenomenon could be due to two possible reasons. One is that the peak force driven by the pulsatile pressure can break up more plasma bridges of blood cells and so reduce the blood viscosity in PVBs. The other is that the peak force may also dilate the caliber of the precapillary opening. These two benefits, one reduces the blood viscosity and the other reduces the resistance of the precapillary opening, can assist blood perfusion in PVBs.

In the region where BPPI is larger than 0.69, the FPARs of the larger parts greatly increase. The increasing rate of the peak part (FPAR I) is much faster than the others. On the other hand, the FPAR of the lowest part is almost constant (Fig. 4 and Table 3). Similar to the movement from rest of an object with a large static frictional force, in the transition when starting to move, a large peak force is necessary to overcome the static frictional force. In the moving phase, the kinetic frictional force is almost constant and smaller than the static force. Most of the driving force, except that reduced by the kinetic frictional force, can easily accelerate the movement. When the peak force exceeds a threshold, it can break up most of the blood-cell interlinkings in PVBs, and the RBCs could be easily deformed to pass through the small vessels. It had been reported that blood viscosity is reduced as shear rate increases, tending to an asymptotic value as the rate of shear exceeds a threshold [24]. Furthermore, due to the properties of some active components, the dilation and the elongation of smooth muscle are complex and relate to its excitation force and initial condition [25, 26]. A larger peak force could vastly dilate the precapillary opening, which could increase both the blood perfusion velocity and the area of the perfusion channel.

The passive factor of the driven blood flow is mainly dependent on the blood viscosity and the diameter of the upstream vessel. In PVBs, as the blood cells or their aggregations are larger than the diameter of the blood vessels, flow through these vessels will be more resistive. Without sufficient driving force, the blood cells may not be deformed so as to be able to squeeze through the vessels but instead obstruct them. When this occurs, a large peak force can either dilate the vessel so as to dislodge the obstruction or break up the aggregation and deform the RBCs so that they can pass through the vessels. When vessels in the PVBs become stiffer, they become harder to dilate and to increase the shear rate. Thus, in order to maintain constant perfusion, a larger force is needed to dilate the stiffer vessels as well as to increase the shear rate.

The results show that the higher the PBP, the greater the driven flux. There appears to be a threshold of BPPI, above which the driving efficiency would be amplified abruptly (Fig. 4). This implies that pulsatility plays a role in lowering the resistance of PVB vessels as well as in regulating blood pressure in large arteries.

Authorized licensed use limited to: National Taiwan University. Downloaded on August 02,2022 at 06:45:49 UTC from IEEE Xplore. Restrictions apply.

Conclusions

This study shows that the higher-frequency components of the PBP can perfuse blood flux in PVBs more efficiently. As a result, we further infer that if the precapillary openings are obstructed or if the peripheral blood vessels become stiffer, the pulsatile pressure will become higher so as to maintain perfusion. This higher driving pressure could be manifested as the condition we recognize as essential systemic hypertension.

Ming-Yie Jan received the B.S. degree in electrical engineering at Tatung University (1991) and the M.S. degree in biomedical engineering at National Yang-Ming University (1993). He received his Ph.D. in biomedical engineering from the Institute of Electrical Engineering, National Taiwan University, in January 2000. He has been a student member of IEEE since 1998.

Hsin Hsiu received the B.S. degree (1993) and the M.S. degree (1995) in electrical engineering at the National Taiwan University. He is currently a Ph.D. candidate in the Biomedical Engineering Group, Institute of Electrical Engineering, National Taiwan University.

Tse-Lin Hsu received the B.S. degree (1977) in physics from National Tsin-Hua University and the M.S. degree (1979) in biophysics from New York State University at Buffalo. She has been a research analysis fellow of the Biophysics Laboratory, Institute of Physics, Academia Sinica, since 1981.

Yuh-Ying Lin Wang received the B.S. degree in physics from National Taiwan University in 1969 and the M.S. (1971) and Ph.D. (1974) degrees at the University of Maryland. She has been an associated professor and professor in the Department of Physics at the National Taiwan Normal University since 1975.

Wei-Kung Wang received the B.S. degree in physics from National Taiwan University in 1966, the M.S. from National Tsin-Hua University (1971), and the Ph.D. in biophysics from John Hopkins University. He served as professor and director of the Institute of Biomedical Engineering at National Yang-Ming University from 1985-1987. He has been a professor in the Department of Electrical Engineering at National Taiwan University and research fellow of the Biophysics Laboratory, the Institute of Physics, Academia Sinica (joint appointment), since 1988.

Address for Correspondance: W.K. Wang, Biophysics Lab, Institute of Physics, Academia Sinica, Taipei, Taiwan, R.O.C. Tel: +886 2 27899626. Fax: +886 2 27834187. E-mail: wkwang@phys.sinica.edu.tw.

References

1. **Camm AJ:** Cardiovascular disease. In: Kumar P, Clark M (Eds): *Clinical Medicine*. 4th Ed. London: W.B. Saunders, 1998.

2. **Zweifach BW:** Quantitative studies of microcirculatory structure and function. I. Analysis of pressure distribution in the terminal vascular bed in cat mesentery. *Cir Res* 34: 843-857, 1974.

3. **Nichols WW and O'Rourke MF:** *McDonald's Blood Flow in Arteries*. 3rd Ed. London: Edward Arnold, 1990.

4. **Chabanel A and Chien S:** Blood viscosity as a factor in human hypertension. In: Laragh JH, Brenner BM (Eds): *Hypertension: Pathophysiology, Diagnosis, and Management*. 2nd Ed. New York: Raven Press Ltd., ch. 22, 1995.

5. **Cokelet GR:** Rheology and hemodynamics. *Annu Rev Physiol* 42: 311-324, 1980.

6. **Pries AR, Secomb TW, and Gaehtgens P:** Biophysical aspects of blood flow in the microvasculature. *Cardiovasc Res* 32: 654-667, 1996.

7. **Hochmuth RM:** Properties of red blood cells. In: Skalak R, Chien, S (Eds): *Handbook of Bioengineering*. New York: McGraw-Hill, ch. 12, 1987.

8. **Zadar PR, Chien S, Skalak R:** Interaction of a viscous incompressible fluid with an elastic body. In: Belytschko T, Geers TL (Eds): *Computational Methods for Fluid-Structure Interaction Problems*. New York: Springer-Verlag, pp. 365-376, 1977.

9. **Song H and Tyml K:** Evidence for sensing and integration of biological signals by capillary network. *Am J Physiol*, 265: H1253-H1242, 1993.

10. **Wang Lin YY, Chang CC, Chen JC, Hsiu H, and Wang WK:** Pressure wave propagation in arteries: A model with radial dilatation for simulating the behavior of a real artery. *IEEE Eng Med Biol Mag* 16(1): 51-56, 1997.

11. **Wang Lin YY, Chang SL, Wu YE, Hsu TL, and Wang WK:** Resonance, the missing phenomena in hemodynamics. *Cir Res* 69: 51-56, 1991.

12. **Wang WK, Hsu TL, Chen HL, Jan MY, and Wang Lin YY:** Blood pressure and velocity relation in tissue. In: Leipsh (Ed): *Proc 3rd Int Symp Biofluid Mechanics* pp. 119-132, 1994.

13. **Jan MY, Hsu TL, Wang Lin YY, and Wang WK:** A cyclocorrelogram to analyse the fast laser-Doppler flowmetry. In *Proc World Congress on Medical Physics and Biomedical Engineering* p. 626, 1997.

14. **Jan MY, Huang CY, and Wang WK:** The fast propagating pulsatile blood pressure wave drives the pulsatile renal microcirculation. In *10th Int Congress of Biorheology & 3rd Int Conf on Clinical Hemorheology*, 1999.

15. **Jan MY, Shyu JJ, Hsiu H, Lin Wang YY, and Wang WK:** Coherence between the pulsatile aortic blood pressure and the renal cortical flux in dogs. *Am J Physiol*, to be published.

16. **Holstein-Rathlou NH and Marsh DJ:** Renal blood flow regulation and arterial pressure fluctuation: A case study in nonlinear dynamics. *Physiol Rev* 74(3): 637-681, 1994.

17. **Lipowsky HH:** Mechanics of blood flow in the microcirculation. In: Skalak R, Chien S (Eds): *Handbook of Bioengineering*. New York: McGraw-Hill, 1987.

18. **Gross JF:** The significance of pulsatile microhemodynamics. In: Kaley G and Altura BM (Eds): *Microcirculation*. Vol I. Baltimore: University Park Press, pp. 365-390, 1977.

19. **Lee JJ, Tyml K, Menkis AH, Novick RJ, and Mckenzie FN:** Evaluation of pulsatile and nonpulsatile flow in capillaries of goat skeletal muscle using intravital microscopy. *Microvasc Res* 48: 216-327, 1994.

20. **Fagrell B, Fronek A, and Intaglietta M:** A microscope-television system for studying flow velocity in human skin capillaries. *Am J Physiol* 233(2): H318-H321, 1977.

21. **Schmid-Schonbein GW:** Rheology of leukocytes. In: Skalak R, Chien S (Eds): *Handbook of Bioengineering*. New York: McGraw-Hill, ch. 13, 1987.

22. **Skalak R and Zhu C:** Rheological aspects of red blood cell aggregation. *Biorheology* 27: 309-325, 1990.

23. **Bonner RF and Nossal R:** Principles of laser-Doppler Flowmetry. In: Shepherd AP, Oberg PA (Eds): *Laser-Doppler Blood Flowmetry*. Norwell: Kluwer Academic Publishers, ch. 2, 1989.

24. **Whitmore RL:** *Rheology of the Circulation*. Oxford: Pergamon Press, 1968.

25. **Canfield TR and Dobrin PB:** Static elastic properties of blood vessels. In: Skalak R, Chien, S (Eds): *Handbook of Bioengineering*. New York: McGraw-Hill, ch. 16, 1987.

26. **Milnor WR:** *Hemodynamics*. 2nd Ed. Baltimore: Williams & Wilkins, 1989.

Authorized licensed use limited to: National Taiwan University. Downloaded on August 02,2022 at 06:45:49 UTC from IEEE Xplore. Restrictions apply.